Comparison on physical, chemical, and adsorption properties of activated carbon derived from different solid wastes

Yuan Gao, Qinyan Yue*, Baoyu Gao

Shandong Provincial Key Laboratory of Water Pollution Control and Resource Reuse, School of Environmental Science and Engineering, Shandong University, Jinan 250100, China, Tel. +86 15169056115; email: gy_1988@aliyun.com (Y. Gao), Tel. +86 531 88365258; Fax: +86 531 88364513; email: qyyue58@aliyun.com (Q. Yue), Tel. +86 531 88366771; email: baoyugao_sdu@aliyun.com (B. Gao)

ABSTRACT

Four activated carbons (ACs) were prepared from four different solid wastes (SWs), including *Enteromorpha prolifera*, Kraft lignin, hair, and petroleum coke, using KOH as the activating agent. The fabricated ACs were characterized by N_2 adsorption, scanning electron microscopy, transmission electron microscopy, X-ray diffraction, Fourier transformed infrared and X-ray photoelectron spectroscopy to compare their pore structures and surface chemical properties of the ACs. It was found that ACs produced from *E. prolifera* and Kraft lignin were rich in mesopores, whereas petroleum coke and hair were inclined to produce ACs with more micropores. Meanwhile, ACs derived from *E. prolifera* possessed the largest surface area of 3,471 $m^2 \, g^{-1}$ and pore volume of 2.681 $cm^3 \, g^{-1}$. In addition, ACs prepared from various SWs displayed different chemical nature. Adsorption behavior of hexavalent chromium on the four fabricated ACs was studied as well, and the adsorption data were all well fitted by Freundlich equation, indicating the similar multilayer adsorption behavior of hexavalent chromium on the heterogeneous surface of the ACs.

Keywords: Solid waste; Activated carbon; Physicochemical properties; Adsorption; Hexavalent chromium

1. Introduction

With the rapid development of society economy, the growth of human population and the acceleration of urbanization, solid wastes (SWs) generated from the industrial manufactures, agricultural residuals as well as household activities are constantly increasing over million tons [1,2]. According to the statistical data, the annual generation of municipal SWs in China is estimated to reach 200 million tons by 2020 [1,2]. These solids wastes inevitably result in the pollution of soil, water, or air, and further impact the health of human. As a consequence, to find out a proper treatment method is an important and urgent task for the environmental workers. Recently, various methods such as incineration, gasification, anaerobic digestion, composting, and bio-landfilling have been utilized for the dispose of SWs [3]. Among these methods, pyrolysis of SWs is considered as a highly effective waste-to-energy process.

Activated carbons (ACs) produced through SWs pyrolysis have been widely used in many fields, such

*Corresponding author.

as wastewater treatment [4], energy storage [5], gas separation [6], and catalyst supporter [7]. Up to now, a great number of SWs have been converted into the ACs successfully, including orange peel [8], larch sawdust [9], bamboo [10], lotus stalk [11], bio-diesel waste [12], and sugarcane [13]. The species of SWs have significant influence on the physical and chemical characteristics of the ACs. Petroleum coke, a by-product of the oil refinery, has relatively high carbon content (>80 wt%) [14]. *Enteromorpha prolifera*, one kind of marine green alga, is mainly composed of polysaccharide, protein, lipid as well as some mineral salts [15]. Kraft lignin, a woody residual material from cellulose pulping process, has a feature structure of highly cross-linked heterogeneous polymer [16]. Hair, a filamentous biomaterial, is primarily formed of protein, notably large amounts of keratins, which contain five main elements: carbon, oxygen, nitrogen, hydrogen, and sulfur [17]. All four SWs have been proved to be effective, low-cost and widely available starting materials for the synthesis of the ACs [14–17]. However, these SWs possess totally different structure characteristics, which may produce carbons with various properties. Up to now, the reported studies were only focused on the investigations of the effects of the preparation parameters on the final products or the adsorption behavior of the resultant carbons. To the best of our knowledge, there is no discussion involving in the comparison of the properties of AC from totally different SWs.

Therefore, the main objective of this study was to investigate the impacts of different starting materials on physical, chemical nature, and adsorption behaviors of the derived ACs. The physicochemical properties of the ACs were characterized by BET, scanning electron microscopy (SEM), transmission electron microscopy (TEM), FTIR, and X-ray photoelectron spectroscopy (XPS). The effect of experimental variables on the hexavalent chromium adsorption process, such as adsorbent type, adsorbent dosage, and contact time, was studied.

2. Experimental

2.1. Chemicals and materials

Four types of SWs were employed to prepare ACs: coke, lignin, wool, and algae. Petroleum coke was obtained from a petrochemical enterprise (Jinan, China). Kraft lignin was sourced from a papermaking factory (Linyi, China). Hair was obtained from a barbershop (Jinan, China). *E. prolifera* was collected from the shore of the Bohai Sea (Qingdao, China). The raw materials were dried and milled into powders of

0.425 mm. The proximate analysis of Kraft lignin and *E. prolifera* can be found in our previous studies [18,19]. The proximate analysis of petroleum coke and hair is listed in Table 1. The proportion of the organic compound for four materials was in the range between 59.45 and 99.55%, indicating that these waste materials could serve as promising candidates for the synthesis of ACs.

2.2. AC preparation

The raw materials were carbonized at 500°C for 1.5 h using an electric resistance furnace (KSY-4D-16). The heating rate was 10°C min⁻¹. Then, 15 g of the char was directly mixed with KOH powder at a weight ratio of 2.5 (KOH/char). The mixture was activated at 800°C for 1 h in N_2. The heating rate was 20°C min⁻¹. Next, the resultant samples were washed, dried in a vacuum oven, and stored in a desiccator. To reduce error, the preparation experiments were carried out four times and the average values were obtained. The ACs derived from petroleum coke, *E. prolifera*, lignin, and hair are named as PAC, EAC, LAC, and HAC.

2.3. Characterization

2.3.1. Thermal analysis

In order to extract the information on the various thermal behaviors of different SWs during the carbonization process, TGA–DTG analysis was performed using a thermogravimetric analyzer (SHI-MADZU, TGA-50).

2.3.2. Pore distribution analysis

The surface area and pore distribution were determined from the nitrogen adsorption–desorption isotherms using a surface area analyzer (JW-BK122W). Before analysis, all samples were degassed at 300°C for 2 h under vacuum. The surface area was computed according to the BET method. The single-point total pore volume was determined in accordance with the amount of nitrogen adsorption at a relative pressure of 0.99. The micropore volume was calculated by *t*-plot method. The mesopore size distribution was estimated by BJH method.

2.3.3. Morphology analysis

SEM images were obtained using a JEOL, JSM 7600F electron microscope operated at 5.0 kV. TEM

Table 1
Properties of petroleum coke and hair

Sample	Volatile matter (wt%)	Organic compound (wt%)	Ash (wt%)	Moisture (wt%)	Fixed carbon (wt%)
Petroleum coke	11.38	96.48	0.68	0.95	86.99
Hair	77.68	99.55	0.62	9.44	12.26

was performed on a JEM-1011 instrument operated at 100 kV to investigate the interphase microstructures of the carbon materials. X-ray diffraction patterns were recorded on a Rigaku D/MAX-YA diffractometer with Cu Kα radiation in 2θ range from 10° to 70°.

2.3.4. Surface chemistry analysis

The surface functional groups of the carbons were recorded by Fourier transformed infrared spectroscopy (Avatar 370). To further detect the surface chemical properties, XPS was conducted by an ESCA-LAB 250 XPS machine equipped with Al Kα X-ray radiation. The data were standardized to the C1s level at 284.6 eV. XPSPEAK41 software was employed for the peak fitting using shirley-type background subtraction procedure [10,20].

2.4. Adsorption experiments

In kinetic experiments, the ACs of 50 mg were placed to a 50 mL of Cr(VI) solution (50 mg L^{-1}) in conical flask. The samples were withdrawn at a predetermined time interval, filtered, and analyzed for Cr(VI) as a function of time. The concentration of Cr(VI) was determined using a UV analyzer at the maximum absorption wavelength λ_{max} = 540 nm according to 1,5-diphenylcarbohydrazide spectrophotometric method.

The isotherm experiments were carried out using different Cr(VI) concentrations ranging from 20 to 150 mg L^{-1}. Adsorbents in amounts ranging from 0.2 to 3 g L^{-1} were added into 50 mL of Cr(VI) solution. The samples were shaken at 170 rpm for 24 h to guarantee the equilibrium with a thermostatic water bath oscillator (SHA-B, Shanghai, China). Each experiment was performed at room temperature. All experiments were carried out in triplicate and the average values were discussed.

2.5. Adsorption models

The pseudo-first-order model (Eq. (1)), pseudo-second-order model (Eq. (2)), and intra-particle diffusion model (Eq. (3)) are used to investigate the adsorption kinetic behavior.

$$q_t = q_e(1 - e^{-k_1 t}) \tag{1}$$

$$q_t = \frac{q_e^2 k_2 t}{1 + q_e k_2 t} \tag{2}$$

$$q_t = k_{pi} t^{1/2} + C \tag{3}$$

where q_e and q_t are the amount of Cr(VI) adsorption capacity at equilibrium and time t (mg g^{-1}); k_1 is the pseudo-first-order rate constant (min^{-1}); k_2 is the second-first-order rate constant (mg (g min)$^{-1}$); k_{pi} is the intra-particle rate diffusion constant (mg g^{-1} min$^{1/2}$); and C is the constant, which is proportional to the thickness of boundary layer (mg g^{-1}).

To effectively assess the ACs' adsorption capacity, Langmuir isotherm (Eqs. (4) and (5)), Freundlich isotherm (Eq. (6)), and Dubinin–Radushkevich isotherm (Eqs. (7)–(9)) models were used to fit the isotherm data.

$$\frac{C_e}{q_e} = \frac{1}{Q_m b} + \frac{1}{Q_m} C_e \tag{4}$$

$$R_L = \frac{1}{1 + bC_0} \tag{5}$$

$$\log q_e = \log K_F + (1/n) \log C_e \tag{6}$$

$$\ln q_e = \ln q_s - k_{ad} \varepsilon^2 \tag{7}$$

$$\varepsilon = RT \ln(1 + 1/C_e) \tag{8}$$

$$E = 1/(2k_{ad})^{1/2} \tag{9}$$

where C_e is the concentration of Cr(VI) at equilibrium (mg L^{-1}); Q_m (mg g^{-1}) and b (mg L^{-1})$^{-1}$ are the parameters in the Langmuir equation; C_0 is the Cr(VI) initial concentration (mg L^{-1}); and R_L, a dimensionless constant, is defined by Foo and Hameed [21]. K_F (mg g^{-1}) ((mg L^{-1})$^{n-1}$)$^{-1}$ and n are parameters in the Freundlich equation. q_s is the theoretical saturation capacity in the Dubinin–Radushkevich equation (mg g^{-1}); k_{ad} is a constant related to the free energy of

adsorption ($mol^2 kJ^{-2}$); T is the solution temperature (K); and E is the mean free energy (kJ mol^{-1}), which is useful for estimating the adsorption type [22].

3. Results and discussion

3.1. TGA–DTG analysis

As illustrated in Fig. 1, the decomposition of *E. prolifera* and hair was significant between 220 and 500°C. In this stage, the sharp weight losses were 47.3 and 67.3% for *E. prolifera* and hair, respectively. The decomposition of lignin was significant in the whole temperature between 30 and 500°C and the weight loss was 43.8%. However, the petroleum coke only exhibited a slight weight loss of 6.36% in the whole temperature range. Because petroleum coke was the carbonaceous solid by-product of the oil refinery, its decomposition mechanism was different from the

others. The DTG curves display the first peak at 75, 95, 95°C for *E. prolifera*, lignin, and hair, indicating the lost of the external water. Another obvious peak occurred at 237, 335, and 328°C for *E. prolifera*, lignin, and hair, respectively. The obvious difference in thermal behavior was related to the structure or composition of four raw materials.

3.2. Characterization of AC

3.2.1. Surface area and pore structure

Fig. 2(a) depicts the N_2 adsorption–desorption isotherms of the ACs. According to IUPAC, the isotherms of PAC and HAC belonged to type I, indicating the existence of abundant micropores and scarcely any meso/macropores. By contrast, the isotherms of EAC and LAC were a composite of type I and type IV with a hysteresis loop of type H2. The initial adsorption
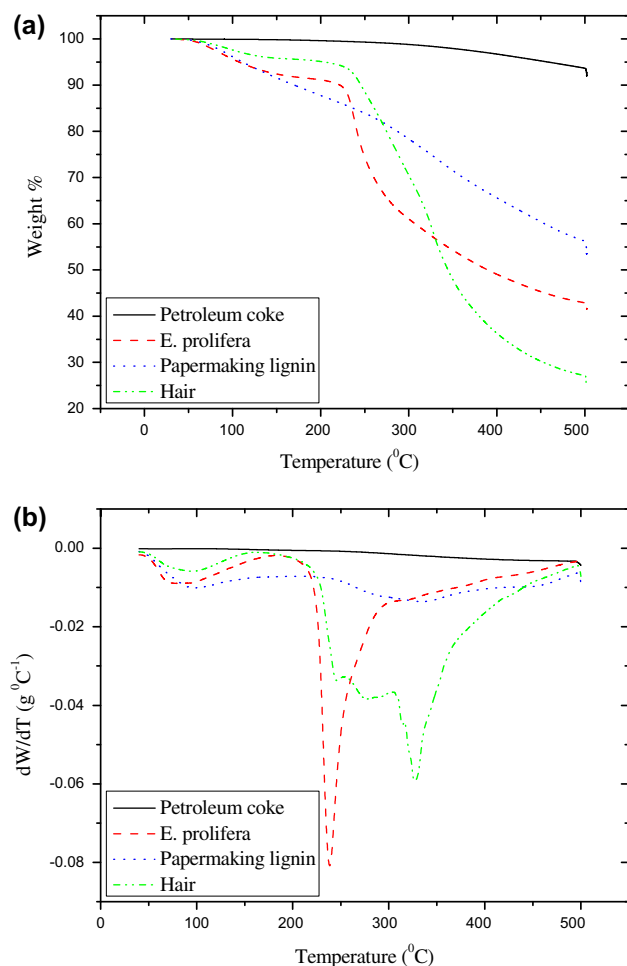
Fig. 1. (a) TGA curves and (b) DTG curves of petroleum coke, *E. prolifera*, lignin of papermaking black liquor and hair during the carbonization process.
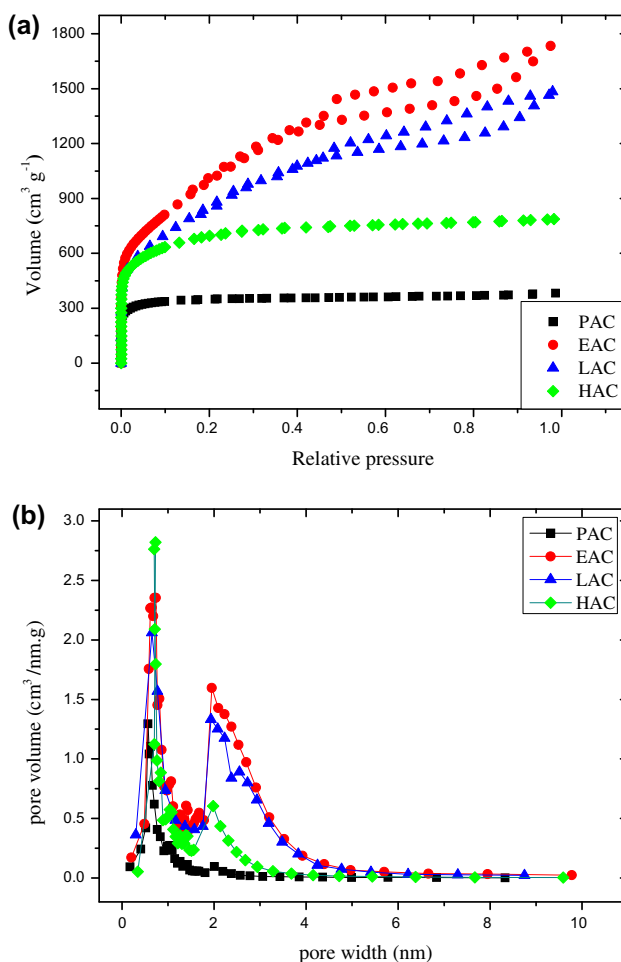
Fig. 2. (a) Nitrogen adsorption–desorption isotherms and (b) pore size distributions of the prepared carbons.

Table 2
Porous structure parameters of the ACs

Sample	S_{BET} (m^2 g^{-1})	S_{mic} (m^2 g^{-1})	S_{BJH} (m^2 g^{-1})	V_{tot} (cm^3 g^{-1})	V_{mic} (cm^3 g^{-1})	V_{mic}/V_{tot} (%)	D_{AC} (nm)
PAC	1,344	1,287	112	0.591	0.520	87.98	1.758
EAC	3,471	1,512	3,004	2.681	0.840	31.33	3.089
LAC	3,119	1,041	2,550	2.296	0.465	20.25	2.943
HAC	2,521	2,253	666	1.218	0.994	81.61	1.932

S_{BET}: BET specific surface area, S_{mic}: micropore internal surface area; S_{BJH}: BJH internal surface area, V_{tot}: total pore volume, V_{mic}: micropore volume, and D_{AC}: mean pore size.

at low relative pressure was due to micropore fillings. The steep adsorption at a relative pressure from 0.5 to 0.9 corresponded to the capillary condensation in the mesopores [8,23]. As shown in Fig. 2(b), the pore size distributions confirm the hierarchical porous structure of these two carbons, containing both micropores (<20 Å) and well-developed mesopores (20–40 Å). The volume of pores with diameters between 20 and 40 Å increased in the order of PAC < HAC < LAC < EAC. The pore of AC can be divided into three types: micropore with pore size diameter less than 20 Å, mesopore with pore size diameter in the range of 20–50 Å, and macropore with pore size diameter larger than 50 Å.

The pores with diameters between 20 and 40 Å belong to mesopore. In general, mesopore was produced by widening the existing micropores. *E. prolifera* is one kind of marine green alga, which is mainly composed of polysaccharide. Kraft lignin is mostly composed of lignin and cellulose. Hair is primarily formed of keratin, and petroleum coke is one kind of coke. Hence, the pyrolysis degree of four raw materials follows an order of petroleum coke < hair < Kraft lignin < *E. prolifera*. In other words, *E. prolifera* is prone to be pyrolyzed and petroleum coke is hard to be pyrolyzed. Thus, the mesopore volume of the obtained AC followed an order of PAC < HAC < LAC < EAC.
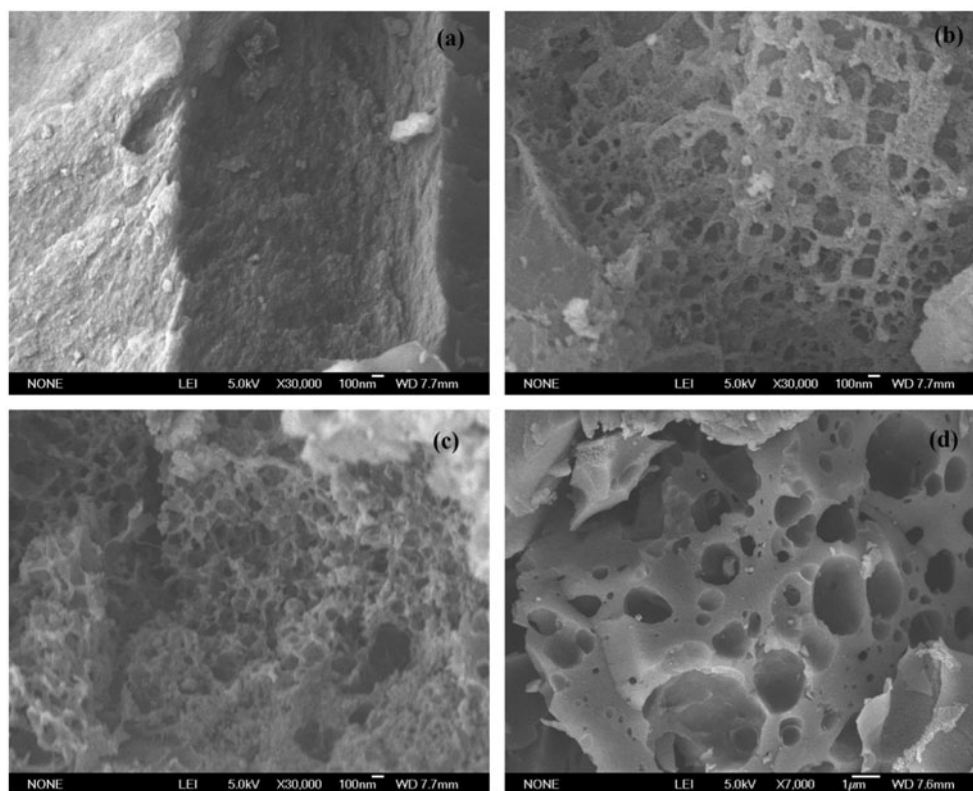
Fig. 3. SEM images of (a) PAC, (b) EAC, (c) LAC, and (d) HAC.
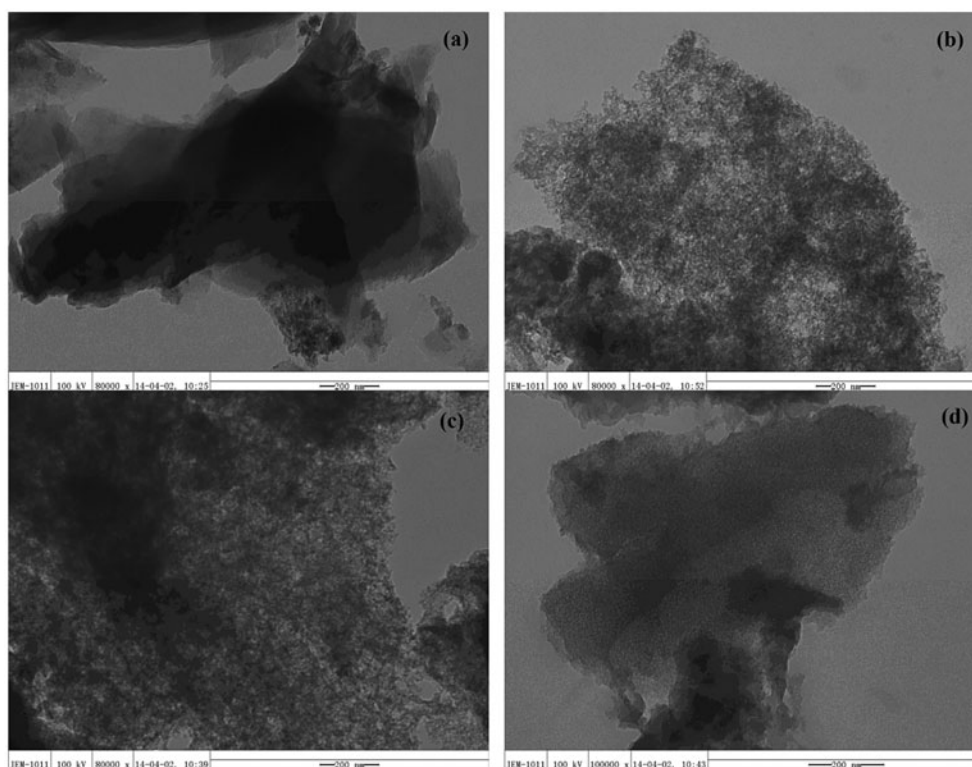
Fig. 4. TEM images of (a) PAC, (b) EAC, (c) LAC, and (d) HAC.

The porous structure parameters of the ACs are listed in Table 2. The porous textures were most developed for EAC (3,471 m^2 g^{-1}), followed by LAC (3,119 m^2 g^{-1}), HAC (2,521 m^2 g^{-1}), and PAC (1,344 m^2 g^{-1}). At the same preparation conditions, ACs produced from lignin and *E. prolifera* were rich in mesopores; however, ACs created from hair and petroleum coke were rich in micropores. The micropore volume occupied only 31.33 and 20.25% of the total pore volume for EAC and LAC, respectively. However, the micropore volume occupied 87.98 and 81.61% of the total pore volume for PAC and HAC, respectively. These significant differences in pore structure may be mainly due to the totally various pyrolysis behaviors of the raw precursors, which can be explained according to the above-mentioned TGA–DTG analysis. The difference in weight loss reflected the degree of pyrolysis of the samples, and the pyrolysis characteristics were closely related to the pore development of a carbon material [24].

3.2.2. Morphology analysis

More surface physical information is illustrated by SEM (Fig. 3) and TEM (Fig. 4). It can be clearly seen that the surfaces of EAC and LAC were more highly developed with different size pores than those of PAC and HAC, which is in accordance with the surface area analysis. The surface of PAC exhibited much smoother than others without any obvious pores. The
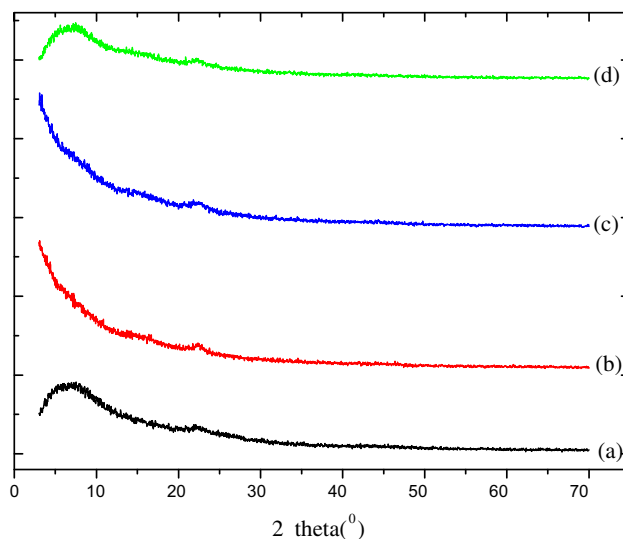
Fig. 5. XRD patterns of (a) PAC, (b) EAC, (c) LAC, and (d) HAC.

Table 3
Peak assignment of C1s, O1s, N1s for the prepared carbons

Peak	Binding energy (eV)	Assignment	Relative content (%) PAC	Binding energy (eV)	Assignment	Relative content (%)		
						EAC	LAC	HAC
C1s	282.7	VC	32.46	284.6	C=C	37.31	32.66	32.86
	284.2	C=C	29.99	285.6	C–O, C–N/S	17.48	24.89	18.38
	291.4	π–π^*	2.65	288.5	COO	21.47	14.27	21.19
O1s	529.8	MgO	12.81	531.1	C=O	1.44	5.51	4.89
	531.1	Al_2O_3/C=O	8.99	532.6	C–O–C	13.48	10.89	13.57
				533.5	O=C–O	7.15	8.89	6.03
N1s	397.7	Nitrile N	10.71					
	399.3	Pyrrolic/pyridone N	2.39	399.8	Pyrrolic/pyridine N	1.67	2.89	3.08

Table 4
Estimated kinetic model constants for hexavalent chromium adsorption

Type of the adsorbents	PAC	EAC	LAC	HAC
q_e(exp) (mg/g)	28.917	46.948	46.097	42.525
First-order kinetics				
k_1 (min^{-1})	0.0168	0.0087	0.0092	0.0100
q_e(cal) (mg/g)	19.001	20.145	22.211	21.103
R^2	0.9590	0.9386	0.9417	0.9495
Second-order kinetics				
k_2 (g/mg min)	2.945×10^{-3}	2.220×10^{-3}	1.950×10^{-3}	2.289×10^{-3}
q_e(cal) (mg/g)	29.762	46.948	46.296	42.735
R^2	0.9991	0.9987	0.9986	0.9991
Intra-particle diffusion				
K_{p1} (mg/g min$^{1/2}$)	3.9288	6.6556	5.8310	6.1086
C	2.4899	7.8635	7.3255	4.4506
R^2	0.9429	0.8415	0.8231	0.9227
K_{p2} (mg/g min$^{1/2}$)	0.8992	1.0315	1.0399	0.9082
C	15.583	29.704	28.238	27.443
R^2	0.9755	0.9778	0.8463	0.9569

surface of EAC seemed like a honeycomb-like uninterrupted network with many relatively non-uniform pores. The inner walls of large pores contained some smaller pores. By contrast, the flower cluster-like network with relatively homogeneous pores was observed on the surface of LAC. Some shallow pores with various sizes were presented on the external surface of HAC. To investigate the disorder degree of the porous carbon structures, TEM images are displayed in Fig. 4. EAC and LAC were formed by much higher turbostratic amorphous structure with different dimension and thickness carbon sheets and clusters than PAC and HAC. The image of PAC presented like a panel without any remarkable disordered structure. Fig. 4(d) shows that numerous small and uniform nanopores formed the non-crystalline layered structure of HAC. In addition, the XRD profiles (Fig. 5) of four carbons displayed a diffraction peak around $2\theta = 22°$, corresponding to the (0 0 2) planes [25]. The peak positions of PAC, EAC, LAC, and HAC were 21.94°, 22.48°, 22.24°, and 22.28°, respectively. The peak position for PAC was at a lower angle, which indicated that the disordered degree of amorphous carbon for PAC was lower than those of other carbons [26]. These results are in good agreement with the TEM images.
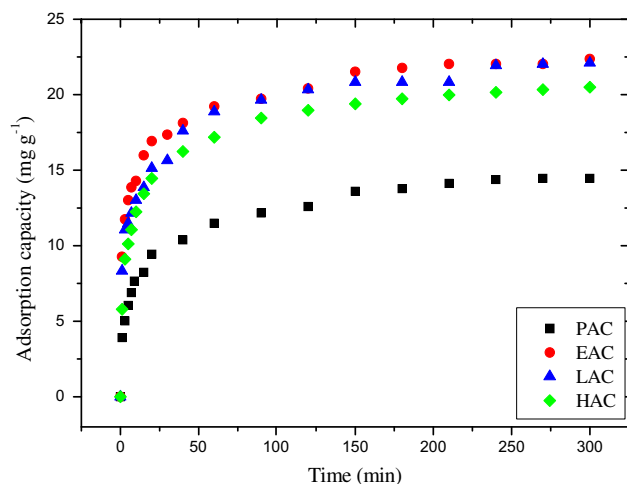
Fig. 6. Adsorption kinetics for the removal of Cr(VI) using four carbons (Cr(VI) = 50 mg L^{-1}, adsorbent dose = 0.05 g/50 mL, stirring speed = 170 rpm, and temperature = 25°C).

3.2.3. Chemical properties analysis

The high-resolution XPS of four carbons revealed different peak locations and proportions (Table 3). For EAC, LAC, and HAC, the spectrum of C1s could be deconvolved into three single peaks. The peaks at around 284.6 eV corresponded to sp^2 hybridized carbon [17]. The peaks at 285.6 eV were assigned to singly bonded carbon atoms to oxygen, nitrogen, or sulfur in the form of phenol, alcoholic, thiophene, or thioether [17,19,27]. The peaks at 288.5 eV were considered as ester or carboxylic group features. The oxygen spectrum revealed three different contributions: C=O (531.1 eV), C–O–C or oxygen atoms in hydroxyl groups (532.6 eV), and O=C–O (533.5 eV) [28]. In the case of PAC, three different types of C-containing groups were verified: including VC, C=C and π–π* transition, corresponding to the peaks at 282.7, 284.2, and 291.4 eV, respectively. The spectrum of O1s revealed two characteristic oxygen states of MgO (529.8 eV) and Al$_2$O$_3$ or C=O (531.1 eV). The ash content of petroleum coke may be composed of some inorganic constituent, such as magnesium, aluminum, calcium, or iron [29,30]. Therefore, Mg or Al doping could be introduced into the resultant carbon products.

3.3. Adsorption of hexavalent chromium

3.3.1. Adsorption dynamics

The influence of contact time of Cr(VI) onto four carbons is presented in Fig. 6. For four adsorbents, the adsorption amount increased drastically in the first 50 min; about 240 min of contact was required to reach equilibrium. In order to guarantee the adsorption equilibrium, the following batch experiments were performed for 24 h. Fig. 6 also presents that EAC and LAC had larger equilibrium uptake than PAC and HAC. As mentioned above, EAC and LAC had higher surface area and pore volume than PAC and HAC.

The sorption of heavy metal ions onto ACs is a complex procedure; hence, the kinetic models were used to investigate the experimental data. The calculated parameters are listed in Table 4. The pseudo-second-order kinetic model was more suitable to represent the kinetic data than other models, due to its higher correlation coefficient and better agreement of q_e values between the calculated data and the experimental one. This result gives an indication that the adsorption rate of Cr(VI) was mainly limited by chemisorption, involving valence forces through exchanging or sharing electrons between the adsorbent and adsorbate, chelation, coordination, or complexation [31,32]. The predicted q_e values based on the pseudo-first-order model were lower than the experimental values, which were probably due to a time lag, caused by the boundary layer or external resistance at the beginning of the sorption process [31].

According to the reported researches [33,34], the adsorption process can be controlled by several steps. The first stage was bulk solution transport, where the adsorbate ions diffused through the solution to the boundary layer around the adsorbent particles; the second stage was film diffusion, where the adsorbate ions passed through the liquid film to the adsorbent
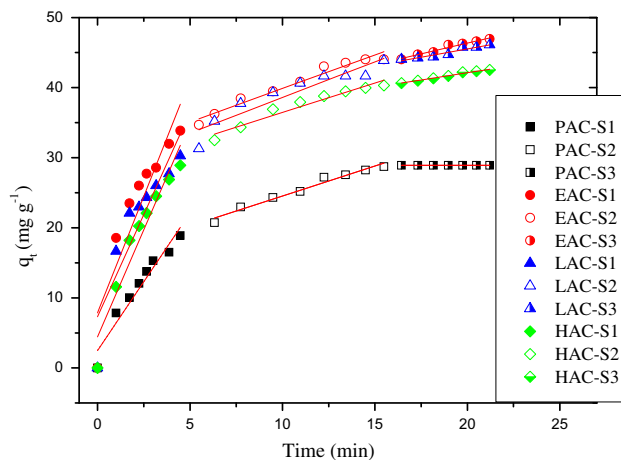
Fig. 7. The intra-particle diffusion plots for the removal of Cr^{6+} using four carbons (Cr(VI) = 50 mg L^{-1}, adsorbent dose = 0.05 g/50 mL, stirring speed = 170 rpm, and temperature = 25°C).
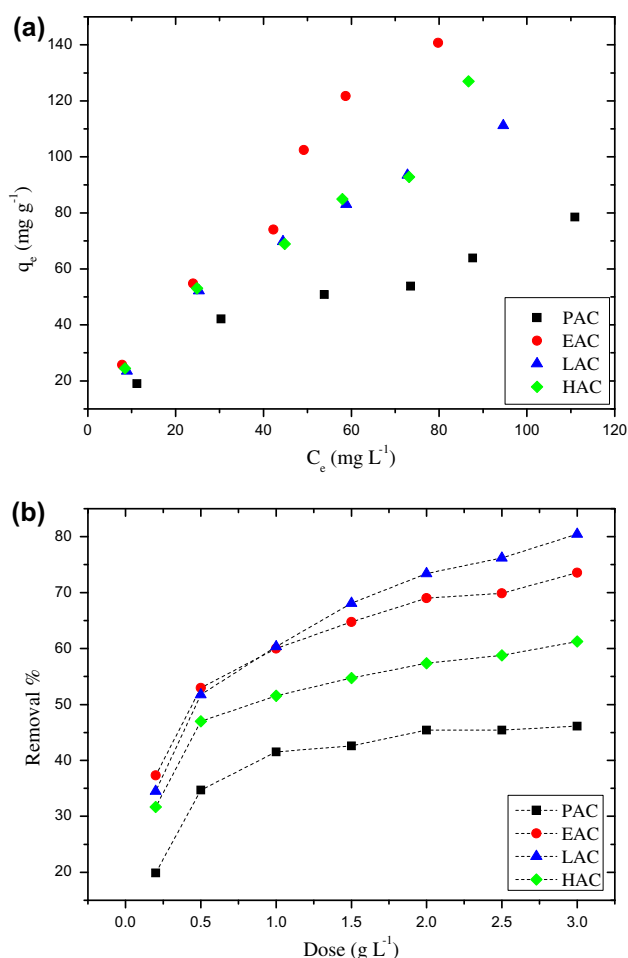
Fig. 8. (a) Adsorption isotherm of Cr(VI) onto four carbons (adsorbent dose = 0.05 g/50 mL, stirring speed = 170 rpm, contact time = 24 h, and temperature = 25℃) and (b) effect of adsorbent dose on chromium removal ([Cr(VI)] = 50 mg L^{-1}, stirring speed = 170 rpm, contact time = 24 h, and temperature = 25℃).

surface; the third stage was pore diffusion, where the adsorbate ions transported to the available adsorption sites. The multiple linear plots (Fig. 7) indicated that more than one process was involved in the adsorption process. The linear plots did not pass though the origin, suggesting the existence of boundary layer resistance between the adsorbate and the adsorbent. The intercept C was ordered from high to low values as EAC > LAC > HAC > PAC, indicating higher boundary layer resistance for EAC and LAC.

3.3.2. Adsorption isotherms

To further understand the adsorption mechanism, one of the most essential data is the adsorption equilibrium isotherms. The isotherms and parameters are

shown in Fig. 8(a) and Table 5. The Freundlich model provided the best fit to the experimental data in comparison with Langmuir and Dubinin–Radushkevich model, signifying the multilayer adsorption of Cr(VI) on the heterogeneous surface of ACs. The Langmuir equation predicted that the maximum monolayer adsorption capacities were 312.5, 178.6, 147.1, and 107.5 mg g^{-1} for EAC, LAC, HAC, and PAC, respectively. This sequence was in accordance with the BET surface area, demonstrating the important role of ACs' surface area in the adsorption capacity. The values of the separation factor R_L were in the range of 0–1, indicating favorable adsorption process for four adsorbents. Smaller value of $1/n$ implied stronger adsorption intensity or more heterogeneous between adsorbent and heavy metal. The lowest $1/n$ value of 0.5708 for PAC suggested the strongest interaction between Cr(VI) ions and AC particles.

3.3.3. Effect of adsorbent dose on the adsorption

In order to predict the treatment cost of resultant carbons per unit of Cr(VI) solution, it is indispensable to discuss the effect of adsorbent dose. For four carbons, the removal rate increased rapidly with the increasing adsorbent dose from 0.2 to 1.0 g L^{-1} (Fig. 8(b)). This was attributed to more availability adsorption sites and stronger driving force with the addition of adsorbent. Further increase of adsorbent dose from 1.0 to 3.0 g L^{-1} resulted in sharp increase in Cr(VI) ion removal rate for HAC, LAC and EAC. However, in the case of PAC, the Cr(VI) ion removal rate almost kept constant with further addition of the adsorbent. It may be due to that the overcrowding of adsorbent particles led to the overlap of many adsorption sites or unsaturation of some exterior surface of adsorbent [35]. Because the raw material for PAC was petroleum coke, PAC exhibited higher grain density than other carbons.

3.3.4. FTIR analysis before and after adsorption

FTIR spectroscopy was used to investigate the vibrational frequency changes in the functional groups of the ACs due to Cr(VI) adsorption. As shown in Fig. 9, the bands at 3,450 cm^{-1} were due to the O–H stretching vibration [36]. The bands at 2,923 cm^{-1} were ascribed to C–H vibration. The bands around 1,625 cm^{-1} corresponded to the stretching vibration of C=O [37]. The bands around 1,105 cm^{-1} were assigned to the C–O stretching vibration in ethers or phenols. After Cr(VI) adsorption onto the ACs, changes in intensity and shifts in position could observed in the

Table 5
Isotherm model constants for hexavalent chromium adsorption onto adsorbents

Isotherms	Constants	Adsorbents			
		PAC	EAC	LAC	HAC
Langmuir	Q_m (mg g^{-1})	107.5	312.5	178.6	147.1
	b (L mg^{-1})	0.0180	0.0102	0.0158	0.0225
	R_L	0.2695	0.3952	0.2959	0.2283
	R^2	0.9136	0.8995	0.9763	0.9809
Freundlich	K_F ((mg L^{-1})$^{n-1}$)$^{-1}$	5.144	5.310	5.942	6.725
	$1/n$	0.5708	0.7553	0.6477	0.6194
	R^2	0.9645	0.9953	0.9942	0.9921
Dubinin–Radushkevich	E (kJ mol^{-1})	0.1291	0.1581	0.1581	0.1581
	q_s (mg g^{-1})	60.27	106.9	85.04	87.24
	R^2	0.8851	0.8174	0.8657	0.8142
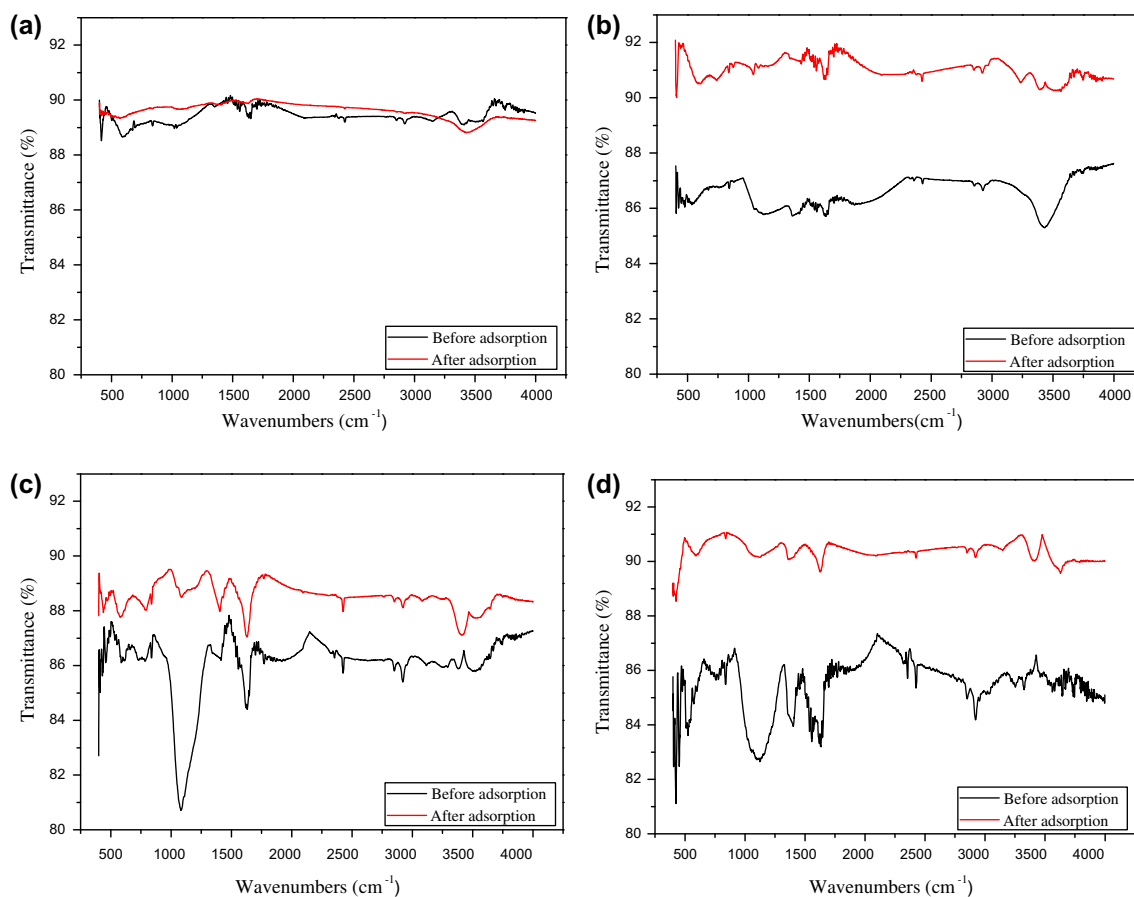
Fig. 9. FTIR spectra of (a) PAC, (b) EAC, (c) LAC, and (d) HAC before and after the adsorption of Cr(VI).

FTIR spectra. For example, the bands around 3,450 and 1,105 cm^{-1} significantly weakened after sorption. Thus, these results implied that the surface functional groups involved in the adsorption processes, which could be found in previous studies [36–39]. The surface chemical properties affected the surface

complexation reaction between the adsorbate ion and adsorbent particle. The surface acidic functional groups of the AC, such as carboxylic, hydroxyl, and carbonyl, play a role in the removal of Cr(VI) in solution. As Cr(VI) exhibited very high positive redox potential (E_0) in the range of 0.68–0.38, which indicated that hexavalent chromium is a strong oxidizer and the surface acidic functional groups could serve as electron donors [38,40]. Thus, Cr(VI) could be reduced Cr(III). In addition, a part of Cr(III) could be removed by ion exchange between the existed hydroxyl and/or carboxyl groups and Cr(III).

4. Conclusions

The physical and chemical properties of ACs (e.g., surface area, pore structure, and surface chemistry) significantly depended on the composition and chemical structure of the raw materials. The BET surface area of the ACs obtained from *E. prolifera*, Kraft lignin, hair, and petroleum coke were 3,471, 3,119, 2,521, and 1,344 $m^2 g^{-1}$, respectively. ACs derived from *E. prolifera* and lignin were rich in mesopores, whereas ACs produced from hair and petroleum coke possessed more micropores. These were due to the more easy decomposition of *E. prolifera* and Kraft lignin compared with petroleum coke and hair under same conditions. ACs produced from petroleum coke displayed different types of C-containing groups in comparison with other three ACs. In addition, as a result of the different physical and chemical properties of the four ACs, adsorption ability toward Cr(VI) varied from each other, but all of which followed the Freundlich model.

References

[1] H. Zhou, A. Meng, Y. Long, Q. Li, Y. Zhang, An overview of characteristics of municipal solid waste fuel in China: Physical, chemical composition and heating value, Renewable Sustainable Energy Rev. 36 (2014) 107–122.

[2] P. Zhao, Y. Shen, S. Ge, Z. Chen, K. Yoshikawa, Clean solid biofuel production from high moisture content waste biomass employing hydrothermal treatment, Appl. Energy 131 (2014) 345–367.

[3] H.A.Arafat,K.Jijakli, A.Ahsan, Environmental performance and energy recovery potential of five processes for municipal solid waste treatment, J. Cleaner Prod. (2013).

[4] M. Kilic, E. Apaydin-Varol, A.E. Pütün, Adsorptive removal of phenol from aqueous solutions on activated carbon prepared from tobacco residues: Equilibrium, kinetics and thermodynamics, J. Hazard. Mater. 189 (2011) 397–403.

[5] T. Sun, F. Xiao, R. Tang, Y. Wang, H. Dong, Z. Li, H. Wang, O. Liuzhang, M. Zhu, Hydrogen storage performance of nano Ni decorated $LiBH_4$ on activated carbon prepared through organic solvent, J. Alloys Compd. 612 (2014) 287–292.

[6] B.S. Caglayan, A.E. Aksoylu, CO_2 adsorption on chemically modified activated carbon, J. Hazard. Mater. 252–253 (2013) 19–28.

[7] S. Baroutian, M.K. Aroua, A.A. Raman, N.M. Sulaiman, A packed bed membrane reactor for production of biodiesel using activated carbon supported catalyst, Bioresour. Technol. 102 (2011) 1095–1102.

[8] M.E. Fernandez, G.V. Nunell, P.R. Bonelli, A.L. Cukierman, Activated carbon developed from orange peels: Batch and dynamic competitive adsorption of basic dyes, Ind. Crops Prod. 62 (2014) 437–445.

[9] W. Li, Z. Huang, Y. Wu, X. Zhao, S. Liu, Honeycomb carbon foams with tunable pore structures prepared from liquefied larch sawdust by self-foaming, Ind. Crops Prod. 64 (2015) 215–223.

[10] Q.-S. Liu, T. Zheng, P. Wang, L. Guo, Preparation and characterization of activated carbon from bamboo by microwave-induced phosphoric acid activation, Ind. Crops Prod. 31 (2010) 233–238.

[11] H. Liu, J. Zhang, N. Bao, C. Cheng, L. Ren, C. Zhang, Textural properties and surface chemistry of lotus stalk-derived activated carbons prepared using different phosphorus oxyacids: Adsorption of trimethoprim, J. Hazard. Mater. 235–236 (2012) 367–375.

[12] S. Kanchi, K. Bisetty, G. Kumar, C.-Y. Lin, T.-S. Chin, Development of green energy waste activated carbon for removal of trivalent chromium: Equilibrium and kinetic modeling, Sep. Sci. Technol. 49 (2014) 513–522.

[13] J. Sreńscek-Nazzal, W. Kamińska, B. Michalkiewicz, Z.C. Koren, Production, characterization and methane storage potential of KOH-activated carbon from sugarcane molasses, Ind. Crops Prod. 47 (2013) 153–159.

[14] N. Rambabu, R. Azargohar, A.K. Dalai, J. Adjaye, Evaluation and comparison of enrichment efficiency of physical/chemical activations and functionalized activated carbons derived from fluid petroleum coke for environmental applications, Fuel Process. Technol. 106 (2013) 501–510.

[15] Y. Li, Q. Du, X. Wang, P. Zhang, D. Wang, Z. Wang, Y. Xia, Removal of lead from aqueous solution by activated carbon prepared from *Enteromorpha prolifera* by zinc chloride activation, J. Hazard. Mater. 183 (2010) 583–589.

[16] C.M. Fierro, J. Górka, J.A. Zazo, J.J. Rodriguez, J. Ludwinowicz, M. Jaroniec, Colloidal templating synthesis and adsorption characteristics of microporous–mesoporous carbons from Kraft lignin, Carbon 62 (2013) 233–239.

[17] W. Si, J. Zhou, S. Zhang, S. Li, W. Xing, S. Zhuo, Tunable N-doped or dual N,S-doped activated hydrothermal carbons derived from human hair and glucose for supercapacitor applications, Electrochim. Acta 107 (2013) 397–405.

[18] Y. Gao, Q.-Y. Yue, Y.-Y. Sun, J.-N. Xiao, B.-Y. Gao, P. Zhao, H. Yu, Optimization of high surface area activated carbon production from *Enteromorpha prolifra* with low-dose activating agent, Fuel Process. Technol. 132 (2015) 180–187.

[19] Y. Gao, Q. Yue, B. Gao, Y. Sun, W. Wang, Q. Li, Y. Wang, Preparation of high surface area-activated carbon from lignin of papermaking black liquor by KOH activation for Ni(II) adsorption, Chem. Eng. J. 217 (2013) 345–353.

[20] A.M. Puziy, O.I. Poddubnaya, R.P. Socha, J. Gurgul, M. Wisniewski, XPS and NMR studies of phosphoric acid activated carbons, Carbon 46 (2008) 2113–2123.

[21] K.Y. Foo, B.H. Hameed, Insights into the modeling of adsorption isotherm systems, Chem. Eng. J. 156 (2010) 2–10.

[22] K. Vijayaraghavan, T.V. Padmesh, K. Palanivelu, M. Velan, Biosorption of nickel(II) ions onto Sargassum wightii: Application of two-parameter and three-parameter isotherm models, J. Hazard. Mater. 133 (2006) 304–308.

[23] Q. Wang, J. Yan, Y. Wang, T. Wei, M. Zhang, X. Jing, Z. Fan, Three-dimensional flower-like and hierarchical porous carbon materials as high-rate performance electrodes for supercapacitors, Carbon 67 (2014) 119–127.

[24] D. Montane, V. Tornefernandez, V. Fierro, Activated carbons from lignin: kinetic modeling of the pyrolysis of Kraft lignin activated with phosphoric acid, Chem. Eng. J. 106 (2005) 1–12.

[25] Y.-B. Tang, Q. Liu, F.-Y. Chen, Preparation and characterization of activated carbon from waste ramulus mori, Chem. Eng. J. 203 (2012) 19–24.

[26] Z. Guo, Q. Zhou, Z. Wu, Z. Zhang, W. Zhang, Y. Zhang, L. Li, Z. Cao, H. Wang, Y. Gao, Nitrogen-doped carbon based on peptides of hair as electrode materials for surpercapacitors, Electrochim. Acta 113 (2013) 620–627.

[27] A.P. Terzyk, The influence of activated carbon surface chemical composition on the adsorption of acetaminophen (paracetamol) in vitro, Colloids Surf., A 177 (2001) 23–45.

[28] R.-L. Liu, W.-J. Ji, T. He, Z.-Q. Zhang, J. Zhang, F.-Q. Dang, Fabrication of nitrogen-doped hierarchically porous carbons through a hybrid dual-template route for CO_2 capture and haemoperfusion, Carbon 76 (2014) 84–95.

[29] M. Bläsing, K. Nazeri, M. Müller, Release of alkali metal, sulphur and chlorine species during high-temperature gasification and co-gasification of hard coal, refinery residue, and petroleum coke, Fuel 126 (2014) 62–68.

[30] W. Huo, Z. Zhou, X. Chen, Z. Dai, G. Yu, Study on CO_2 gasification reactivity and physical characteristics of biomass, petroleum coke and coal chars, Bioresour. Technol. 159 (2014) 143–149.

[31] J. Febrianto, A.N. Kosasih, J. Sunarso, Y.H. Ju, N. Indraswati, S. Ismadji, Equilibrium and kinetic studies in adsorption of heavy metals using biosorbent: A summary of recent studies, J. Hazard. Mater. 162 (2009) 616–645.

[32] J. Yu, M. Tong, X. Sun, B. Li, A simple method to prepare poly(amic acid)-modified biomass for enhancement of lead and cadmium adsorption, BioChem. Eng. J. 33 (2007) 126–133.

[33] S.K. Singh, T.G. Townsend, D. Mazyck, T.H. Boyer, Equilibrium and intra-particle diffusion of stabilized landfill leachate onto micro- and meso-porous activated carbon, Water Res. 46 (2012) 491–499.

[34] Y. Sun, Q. Yue, B. Gao, B. Wang, Q. Li, L. Huang, X. Xu, Comparison of activated carbons from Arundo donax Linn with $H_4P_2O_7$ activation by conventional and microwave heating methods, Chem. Eng. J. 192 (2012) 308–314.

[35] J. Fan, J. Zhang, C. Zhang, L. Ren, Q. Shi, Adsorption of 2,4,6-trichlorophenol from aqueous solution onto activated carbon derived from loosestrife, Desalination 267 (2011) 139–146.

[36] M. Bansal, D. Singh, V.K. Garg, A comparative study for the removal of hexavalent chromium from aqueous solution by agriculture wastes' carbons, J. Hazard. Mater. 171 (2009) 83–92.

[37] L. Zhang, Y. Zhang, Adsorption characteristics of hexavalent chromium on HCB/TiO_2, Appl. Surf. Sci. 316 (2014) 649–656.

[38] N.H. Hsu, S.L. Wang, Y.H. Liao, S.T. Huang, Y.M. Tzou, Y.M. Huang, Removal of hexavalent chromium from acidic aqueous solutions using rice straw-derived carbon, J. Hazard. Mater. 171 (2009) 1066–1070.

[39] L. Ramrakhiani, R. Majumder, S. Khowala, Removal of hexavalent chromium by heat inactivated fungal biomass of *Termitomyces clypeatus*: Surface characterization and mechanism of biosorption, Chem. Eng. J. 171 (2011) 1060–1068.

[40] S. Rangabhashiyam, N. Selvaraju, Adsorptive remediation of hexavalent chromium from synthetic wastewater by a natural and $ZnCl_2$ activated Sterculia guttata shell, J. Mol. Liq. 207 (2015) 39–49.